# The Self-Assembly of Inorganic Mimics of Copper Oxidases and Oxygenases: A Theoretical Study

**Attila Bérces***

**Abstract:** We applied gradient-corrected density-functional and continuum-dielectric theories to calculate the formation energy of $[L_nCu_nO_2]^{n+}$ clusters {L = *N*-permethyl-(1*R*,2*R*)-cyclohexenediamine; $n = 1, 2, 3, 4$} by self-assembly reaction in the gas phase and in $CH_2Cl_2$ solution. The calculated gas-phase energies of formation of the mono-, bi-, tri- and tetranuclear clusters are $-117$, $-74$, $-10$ and $+171$ kJ mol$^{-1}$, respectively, relative to one mole of mononuclear $Cu^{I}L$ complex. The solvation energy contributions to the same reactions in $CH_2Cl_2$ are $-6$, $-70$, $-149$ and $-220$ kJ mol$^{-1}$, while total energies of formation in $CH_2Cl_2$ are $-123$, $-144$, $-159$ and $-49$ kJ mol$^{-1}$, respectively. Under these conditions the trinuclear product is the most stable, consistent with the recent discovery of the $Cu_3O_2$ cluster (A. P. Cole et al. *Science* **1996**, 273, 1849). The electronic structure of $L_3Cu_3O_2^{3+}$ has a $^3E'$ ground state, in the idealised highest symmetry $D_{3h}$ conformation, that is subject to Jahn–Teller distortion with two isoenergetic $C_{2v}$ components of the $^3A_1$ and $^3B_1$ electronic states. The experimentally characterised structure is consistent with the $^3B_1$ ($^3B$ under $C_2$ symmetry) electronic state with one pair of short and two pairs of long Cu–O bonds. The $L_3Cu_3(\mu\text{-}\eta^3\text{:}\eta^3\text{-}O_2)$ isomer also has a stable structure, but it is 162 kJ mol$^{-1}$ higher in energy than its oxo analogue. Bidentate ligands are found to be more favourable than tridentate ones for the energetics of $Cu_n$–$O_2$ clusters; this is consistent with a structural reorganisation of the oxyhemocyanin active site upon oxygen binding. On the basis of these results, the trinuclear $Cu_3O_2$ clusters are unlikely to be formed under biological conditions in multicopper oxidases as stable intermediates. The formation of the $Cu_3O_2$ in the self-assembly reaction is controlled by solvation effects.

**Keywords:** bioinorganic chemistry · copper · density functional calculations · multicopper oxidases · solvent effects

## Introduction

The self-assembly approach to the synthesis of $Cu_n$–$O_2$ clusters from monomeric $LCu^{I}$ complexes and $O_2$ has recently lead to the discovery of inorganic clusters with $Cu_2(\mu\text{-}\eta^2\text{:}\eta^2\text{-}O_2)$-, $Cu_2(\mu\text{-}O)_2$- and $Cu_3(\mu\text{-}O)_2$-core structures, which resemble experimentally characterised or hypothetical intermediates in the copper-catalysed biological activation of dioxygen (Scheme 1). The binuclear enzymes oxyhemocyanin[1] and oxytyrosinase[2] with $Cu_2(\mu\text{-}\eta^2\text{:}\eta^2\text{-}O_2)$ active sites carry and activate dioxygen, respectively, through a two-electron reduction of $O_2$ to peroxide. Inorganic mimics of the oxyhemocyanin, $[L_2Cu_2(\mu\text{-}\eta^2\text{:}\eta^2\text{-}O_2)]^{2+}$ with L = 1,4,7-triisopropyl-1,4,7-triazacyclononane (**1A**) and hydrotris(3,5-diisopropyl-1-pyrazolyl)borate (**2**), have recently been synthesised with the self-assembly approach by Tolman et al.[3] and Kitajima et al.[4], respectively. Tolman and co-workers found that whereas **1A** was obtained in dichloromethane, its $Cu_2(\mu\text{-}O)_2$-core isomer (**1B**) was formed in THF. Further, the two isomers readily interconverted upon changing the solvent.[5] The experimentally observed interconversion between the $Cu_2(\mu\text{-}\eta^2\text{:}\eta^2\text{-}O_2)$- and $Cu_2(\mu\text{-}O)_2$-core isomers supports previous suggestions that such isomerisation is the key step in the biological evolution and activation of the O–O bond.[6]

Most recently, Cole et al. reported the self-assembly synthesis of a trinuclear copper–dioxo cluster, $[L_3Cu_3O_2]^{3+}$ {L = *N*-permethyl-(1*R*,2*R*)-cyclohexenediamine} (**3**) with a $Cu_3(\mu\text{-}O)_2$ core.[7] Although such an intermediate has never been observed, the active site of the fully reduced form of ascorbate oxidase contains a trinuclear copper centre with an average Cu–Cu distance of 4.5 Å that is structurally suitable to accommodate an intermediate with a $Cu_3O_2$-core. Multicopper oxidases, laccase, celluroplasmin and ascorbate oxidase all have a trinuclear copper active site to catalyse the four-electron reduction of $O_2$ to $H_2O$.[8] Although these enzymes have been structurally characterised,[9] the intermediates of dioxygen reduction are not well understood.[10] The synthesis of **3** makes it possible to characterise the $Cu_3O_2$

[*] Dr. A. Bérces
Steacie Institute for Molecular Sciences
National Research Council of Canada
100 Sussex Drive, Ottawa, Ontario, K1A 0R6 (Canada)
Fax: (+1) 613-954-5242
E-mail: attila.berces@nrc.ca

  0947-6539/98/0407-1297 $ 17.50+.25/0 

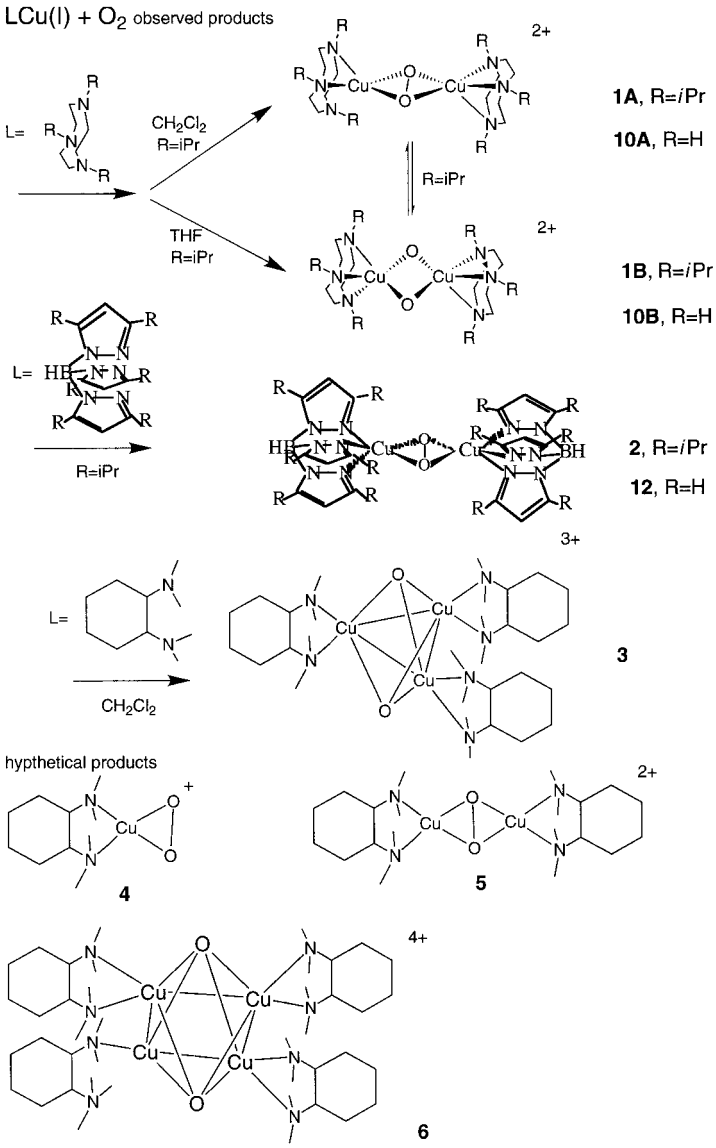


Scheme 1. The possible products of the self-assembly reaction between $Cu^{I}L$ and $O_2$.

chromophore and assist in the identification and detection of such transient forms in biological systems if they exist.

Besides its biological relevance, **3** represents the first example of 3:1 (metal:$O_2$) stoichometry in reactions between metal complexes and dioxygen; these normally proceed with 1:1, 2:1 and 4:1 (metal:$O_2$) stoichometry. To understand the driving forces of the self-assembly reaction that yielded this cluster with an unusual composition, we carried out density-functional calculations for the binding energy of the novel, experimentally observed, trinuclear cluster $[L_3Cu_3(\mu\text{-}O)_2]^{3+}$ {L = *N*-permethyl-(1*R*,2*R*)-cyclohexene-diamine} (**3**) and its mono-, bi- and tetranuclear analogues $[LCuO_2]^{+}$ (**4**), $[L_2Cu_2O_2]^{2+}$ (**5**) and $[L_4Cu_4O_2]^{4+}$ (**6**), respectively. The present calculations are based on density-functional theory (DFT) at generalised gradient approximation (GGA) level and include scalar relativistic corrections in the Hamiltonian (see Computational Details), which have proved to be successful for the calculation of the energetics, structures and spectroscopic properties of transition metal systems.[11] We applied this method to calculate the electronic structure, energetics and properties of inorganic mimics and models of the binuclear copper active site of oxyhemocyanin and oxytyrosinase.[12] Since experimental evidence shows the importance of solvation effects, we augmented the electronic structure calculations with solvation energy calculations based on continuum-dielectric theory.

We were also interested in the qualitative molecular orbital structure of the $Cu_3O_2$ chromophore that can be best studied with the model system $[\{Cu(NH_3)_2\}_3(\mu\text{-}O)_2]^{3+}$ (**7**). Model compounds, such as **7**, can accurately reproduce structural and spectral properties of the $Cu_nO_2$ chromophore of larger inorganic or biological systems and they provide a basis for selecting the ground electronic state.[13] For the accurate calculation of binding energetics the ligands have to be taken into account explicitly; this makes it necessary to optimise the geometry of **3**, **5** and **6** with 107, 72 and 142 atoms and 282, 192 and 372 valence electrons, respectively. Such demanding calculations were made possible by efficient algorithms implemented in the Amsterdam Density-Functional (ADF) program, custom-modified geometry optimisation and parallel computer technology (see Computational Details). The decomposition of the dioxygen binding energy into ligand strain, orbital interaction and steric repulsion components makes it possible to understand the different contributions to the energetics, and to extend some of the conclusions to related biological systems.

## Computational Details

**DFT calculations**: The reported calculations were carried out with the ADF program system, version 2.3, derived from the work of Baerends et al.[14] and developed at the Free University of Amsterdam[15] and at the University of Calgary.[16] All optimised geometries calculated in this study are based on the local density approximation[17] (LDA) augmented with gradient corrections to the exchange[18b] and correlation potentials.[18c] These calculations also include quasirelativistic corrections to the Hamiltonian introduced by Snijders et al.[18] Schreckenbach et al. have implemented the analytical energy gradients based on quasi-relativistic DFT methods.[19] The optimisations were carried out by the direct inversion of iterative subspace for geometry (GDIIS) technique[20] with natural internal coordinates.[21] We have combined the ADF and GDIIS programs[22] and implemented the skeletal internal coordinates.[23] The internal coordinates were generated by the INTC program[24] and augmented by hand.

The atomic orbitals for copper were described by an uncontracted triple-$\zeta$ STO basis set,[25] while a double-$\zeta$ STO basis set was used for carbon, nitrogen, oxygen and hydrogen; a single-$\zeta$ polarisation function was used on all atoms. The $1s^2$ configuration of carbon, nitrogen and oxygen as well as the $1s^22s^22p^6$ configuration of copper were assigned to the core and treated by the frozen-core approximation.[15] A set of auxiliary s, p, d, f, g and h STO functions, centred on all nuclei, was used in order to fit the molecular density and represent the Coulomb and exchange potentials accurately in each SCF cycle.[26]

The numerical integration-accuracy parameter that approximately represents the number of significant digits for the scalar matrix elements was gradually increased to 4.5 until convergence with respect to integration accuracy was reached. This numerical accuracy is sufficient to determine energies within a fraction of a $kJ\,mol^{-1}$ and bond distances within 0.001 Å (which is more accurate than predicted by the definition of the numerical integration-accuracy parameter). The scalable numerical accuracy implemented in the ADF program makes it possible to significantly reduce the computational cost at the initial stages of geometry optimisation when the gradient is still large. These calculations were carried out on a multiprocessor SGI Origin 2000 workstation.



0947-6539/98/0407-1298 $ 17.50+.50/0 *Chem. Eur. J.* **1998**, *4*, No. 7

We did not take into account some effects such as finite temperature, zero-point energy corrections and basis-set superposition error. Most of the error in the final results should be related to these neglected effects and not to error in the DFT energies. Gradient-corrected DFT calculations have repeatedly been shown to provide exceptionally good energetics for transition metal systems.[27]

**Solvation energy calculations**: We fitted a set of point charges to reproduce the electrostatic potential from the density-functional calculations using the total net charge and the dipole moment as constraints with a modified version of the CHELPG program by Breneman and Wiberg.[28] The fitted points lay on a cubic grid between the van der Waals radius and the outer atomic radius with a spacing of 0.2 Å. The outer radii for all atoms are 5 Å, whereas the van der Waals radii for copper, carbon, nitrogen, oxygen and hydrogen are 1.5, 1.7, 1.55, 1.4 and 1.2 Å, respectively. The solvent-reaction field potential due to the fitted ESP charges was calculated by solving the Poisson–Boltzmann equation with the Macroscopic Electrostatics with Atomic Detail (MEAD) program developed by Bashford.[29] In the solvation-energy calculations, the solute molecule within the interior region was assigned a dielectric constant of $\varepsilon_i = 1$, while the outside region was assigned the experimental dielectric constant of the solvent. The solute interior was defined as the region inaccessible to any part of a probe sphere with a radius $r = 2.8$ Å, rolling on the molecular surface of the atomic spheres.

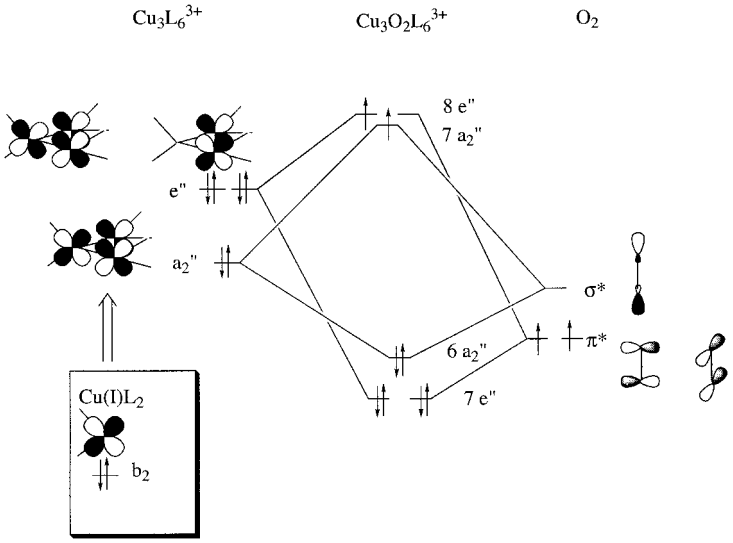


Figure 1. Orbital correlation diagram for $L_3Cu_3O_2^{3+}$.

## Results

**Electronic structure of $L_3Cu_3O_2^{3+}$**: Based on formal electron-counting, the three $Cu^IL$ fragments of complexes **3** and **7** donate a total of four electrons to $O_2$; this gives rise to one $d^8$ and two $d^9$ copper centres. The $d^8$ centre is expected to be low spin, whereas the two $d^9$ centres can interact either ferromagnetically or antiferromagnetically to yield a triplet or a singlet state, respectively. Depending on the strength of the antiferromagnetic interaction, the unpaired electrons of the $d^9$ copper centres can either be localised or delocalised. The localised state can be studied within the single-determinant formalism by the broken symmetry (BS) method combined with spin-projection techniques introduced by Noodleman.[30] We have studied the singlet, triplet and BS states of the $D_{3h}$ and $C_{2v}$ symmetry conformations of **7**. The BS calculations with $C_s$-symmetry restriction on the wavefunction and $C_{2v}$- or $D_{3h}$-symmetry restriction on the geometry initially gave a wavefunction with broken symmetry, but the Cu–Cu distance fell below the bifurcation point during the optimisation, and resulted in a delocalised electronic structure at the optimised geometry.

The discussion of the electronic structure of **7** and the $Cu_3O_2$ chromophore is most conveniently carried out by consideration of the highest $D_{3h}$ symmetry structure; this enables us to correlate the MOs with the σ, σ*, π and π* orbitals of the $O_2$ fragment. Each $Cu^IL_2$ fragment with 14 valence electrons has an occupied high-energy frontier orbital of $b_2$ symmetry[31] that forms a combination of an $a_2''$ and a degenerate pair of e″ orbitals in the $D_{3h}$ conformation of $(CuL_2)_3$ (Figure 1). The $a_2''$ and e″ orbitals can interact with the σ* and π* orbitals, respectively, of the $O_2$ fragment. The density contour plots of the bonding ($6\,a_2''$) and antibonding ($7\,a_2''$) combinations between the σ* $O_2$ orbital and the $a_2''$ CuL-fragment orbitals are shown in Figures 2a and 2b, respectively. The two degenerate components of the $8\,e''$ orbitals (Figures 3a and 3b) are mainly antibonding between the CuL-fragment and the π* $O_2$ orbitals, with anisotropic Cu–O interactions between the individual components. The $8\,e''$ and the $7\,a_2''$ molecular orbitals are close in energy, which gives rise to four different states with small energy separations. The lowest energy $^3E'$ state arises from the occupation of the $7\,a_2''$ orbital by one electron, and one electron shared between the two components of the $8\,e''$ orbital. The next lowest energy state is the $^3A_1'$ with both unpaired electrons residing on the $8\,e''$ orbital. In the lowest energy singlet state ($S_1$), the $7\,a_2''$

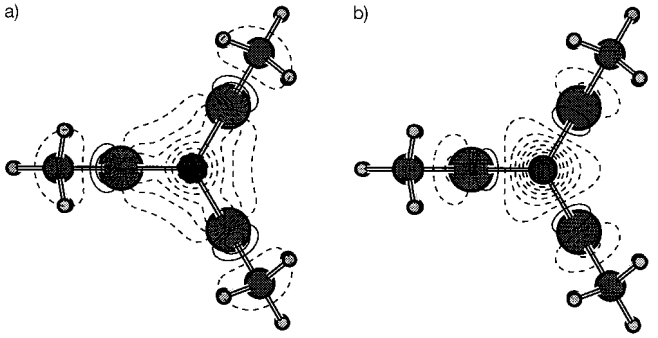


Figure 2. Orbital contour plots of: a) Bonding $6\,a_2''$ orbital; b) antibonding $7\,a_2''$ orbital.

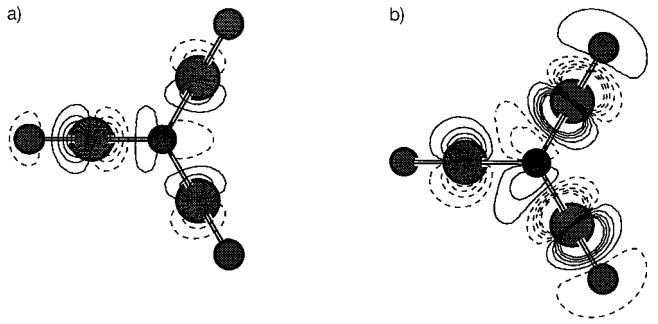


Figure 3. Orbital contour plots of the two degenerate components of the $8e''$ orbital: a) $b_2$ symmetry component; b) $a_2$ symmetry component in $C_{2v}$ point group.

orbital is doubly occupied and the 8e″ level is empty. A higher energy singlet state ($S_2$) arises from the double occupation of the 8e″ level and an unoccupied 7$a_2''$ level.

The fractional occupation of the 8e″ level in the $^3E'$ state makes this lowest energy electron configuration Jahn–Teller unstable. Two isoenergetic $C_{2v}$-symmetric Jahn–Teller components of the $^3A_1$ and $^3B_1$ electronic states arise from the occupation of the $b_2$ (Figure 3a) and the $a_2$ (Figure 3b) components of 8e″ orbital. The $b_2$ component is strongly antibonding between the symmetry-unique copper (Cu2) and the oxygens, whereas it is nonbonding between the two symmetry-related copper atoms (Cu1 and Cu1′) and the oxygens; this explains why this state prefers a geometry with one pair of long and two pairs of short Cu–O bonds. The $a_2$ orbital is strongly antibonding between the symmetry-related copper atoms (Cu1 and Cu1′) and the oxygens. The interaction between the symmetry-unique copper (Cu2) and the oxygens is also antibonding, but it is much weaker due to the smaller overlap between the parallel d- and π-type orbitals. The population of the $a_2$ component yields a preferred geometry with one pair of short and two pairs of long Cu–O bonds.

We carried out calculations on the hypothetical $Cu_3(\mu\text{-}\eta^3\text{:}\eta^3\text{-}O_2)$-core isomers of **3** and **7**, which have similar orbital interactions to the $Cu_3(\mu\text{-}O)_2$ chromophore. The difference between the electronic structures of the $Cu_3(\mu\text{-}\eta^2\text{:}\eta^2\text{-}O_2)$ and $Cu_3(\mu\text{-}O)_2$ chromophores is analogous to the difference found between their binuclear equivalents $Cu_2(\mu\text{-}\eta^2\text{:}\eta^2\text{-}O_2)$ and $Cu_2(\mu\text{-}O)_2$-core.[32] The σ* orbital of the peroxide and the corresponding 7$a_2''$ antibonding orbital are higher in energy than the corresponding levels of the oxo isomer; this leaves the 7$a_2''$ level unoccupied and yields a Jahn–Teller stable $^3A_1'$ ground state.

**Core geometries of $L_nCu_nO_2^{n+}$ clusters**: The optimised bond lengths of different electronic states and conformational isomers of **7** are listed in Table 1. With $D_{3h}$ symmetry the Cu–O bond lengths lie between 1.95 and 1.96 Å for the different electron configurations. The Cu–Cu distances differ more substantially among the different states. The double occupation of the 7$a_2''$ orbital in the $S_1$ state yields the longest Cu–Cu bond length of 2.71 Å, while the shortest Cu–Cu bond of 2.64 Å arises from the occupation of the 8e″ orbitals of the $S_2$ state. The O–O bond lengths of different states of **7** vary between 2.36 and 2.44 Å, while the Cu–N bond lengths lie between 2.02 and 2.06 Å. The two $C_{2v}$-symmetric Jahn–Teller components of the $^3E'$ state of **7** have short and long sets of Cu–Cu, Cu–O and Cu–N bonds. These distances fall within the range found for the $D_{3h}$ conformers with the exception of the Cu–O bonds. For the inorganic system **3** we optimised the geometry of the $^3B$ and $^3E'$ electronic states in the $C_2$- and $D_3$-point groups. In order to study the possible energetic differences between the two Jahn–Teller components in the reduced $C_2$ symmetry, we introduced an intermediate model between **3** and **7**, in which the methyl groups of **3** were replaced by hydrogen atoms (**8**). Table 2 includes the calculated geometries of **3** in $^3B$ and $^3E'$ states and those of **8** in $^3B$ and $^3A$ states.

Table 1. Relative energies [kJ mol$^{-1}$], geometrical parameters [Å], partial charges, spin densities and Hirshfeld charges of $[\{Cu(NH_3)_2\}_3(O_2)]^{3+}$.

| | Exp. | $C_{2v}$ | | $D_{3h}$ | | | |
|---|---|---|---|---|---|---|---|
| electronic state | – | $^3B_2$ | $^3A_1$ | $^3E'$ | $^3A_1'$ | $S_1$ | $S_2$ |
| $E$ [kJ mol$^{-1}$] | – | 0.000 | 0.004 | 0.068 | 0.309 | 0.391 | 0.718 |
| Cu1–Cu2 | 2.705 | 2.761 | 2.715 | 2.725 | 2.678 | 2.730 | 2.665 |
| Cu1–Cu1′ | 2.641 | 2.700 | 2.780 | – | – | – | – |
| Cu1–O | 2.01 | 1.998 | 1.921 | 1.952 | 1.947 | 1.956 | 1.946 |
| Cu1–O | 1.98 | 1.998 | 1.921 | 1.952 | 1.947 | 1.956 | 1.946 |
| Cu2–O | 1.83 | 1.895 | 2.024 | – | – | – | – |
| O–O | 2.37 | 2.293 | 2.295 | 2.309 | 2.366 | 2.315 | 2.383 |
| Cu1–N1 | 2.01 | 2.029 | 2.002 | 2.015 | 2.027 | 1.998 | 2.029 |
| Cu1′–N1′ | 2.04 | 2.029 | 2.002 | 2.015 | 2.027 | 1.998 | 2.029 |
| Cu2–N2 | 1.95 | 1.986 | 2.039 | – | – | – | – |
| qCu1 | – | 0.77 | 0.88 | 0.83 | 0.83 | 0.83 | 0.83 |
| qCu2 | – | 0.96 | 0.75 | – | – | – | – |
| qO | – | −0.72 | −0.72 | −0.72 | −0.72 | −0.72 | −0.73 |
| $q_{(\alpha-\beta)}$Cu1 | – | 0.38 | 0.16 | 0.26 | 0.31 | – | – |
| $q_{(\alpha-\beta)}$Cu2 | – | 0.02 | 0.44 | – | – | – | – |
| $q_{(\alpha-\beta)}$O | – | 0.47 | 0.48 | 0.48 | 0.28 | – | – |
| Hirshfeld | | | | | | | |
| qCu1 | – | 0.49 | 0.46 | 0.48 | 0.48 | 0.48 | 0.47 |
| qCu2 | – | 0.46 | 0.51 | | – | – | – |
| qO | – | −0.29 | −0.29 | −0.29 | −0.29 | −0.32 | −0.29 |

Table 2. Geometrical parameters [Å], partial charges, spin densities and Hirshfeld charges of $[\{CuL\}_3(O_2)]^{3+}$, L = *N*-permethyl-(1*R*,2*R*)-cyclohexenediamine (**3**), L = (1*R*,2*R*)-cyclohexenediamine (**8**).

| | Exp.[a] | **3**, $C_2$ | **3**, $D_3$ | **8**, $C_2$ | **8**, $C_2$ |
|---|---|---|---|---|---|
| electronic state | – | $^3B$ | $^3E$ | $^3B$ | $^3A$ |
| Cu1–Cu2 | 2.705 | 2.654 | 2.701 | 2.736 | 2.675 |
| Cu1–Cu1′ | 2.641 | 2.684 | – | 2.639 | 2.727 |
| Cu1–O | 2.01 | 1.974 | 1.955 | 1.981 | 1.918 |
| Cu1–O | 1.98 | 1.973 | – | 1.987 | 1.918 |
| Cu2–O | 1.83 | 1.911 | – | 1.888 | 2.009 |
| O–O | 2.37 | 2.405 | 2.359 | 2.335 | 2.341 |
| Cu1–N1 | 2.01 | 2.063 | 2.045 | 2.033 | 2.006 |
| Cu1′–N1′ | 2.04 | 2.060 | – | 2.034 | 2.002 |
| Cu2–N2 | 1.95 | 2.050 | – | 1.990 | 2.045 |
| qCu1 | – | 0.67 | 0.70 | 0.69 | 0.78 |
| qCu2 | – | 0.74 | 0.70 | 0.85 | 0.67 |
| qO | – | −0.77 | −0.75 | −0.73 | −0.73 |
| $q_{(\alpha-\beta)}$Cu1 | – | 0.32 | 0.25 | 0.35 | 0.17 |
| $q_{(\alpha-\beta)}$Cu2 | – | 0.17 | 0.25 | 0.07 | 0.43 |
| $q_{(\alpha-\beta)}$O | – | 0.26 | 0.40 | 0.45 | 0.45 |
| Hirshfeld | | | | | |
| qCu1 | – | 0.45 | 0.46 | 0.43 | 0.45 |
| qCu2 | – | 0.46 | 0.46 | 0.47 | 0.42 |
| qO | – | −0.31 | −0.31 | −0.33 | −0.33 |

[a] Ref. [8].

We selected the ground electronic states and the most stable core isomers of the mono-, bi-, tetranuclear analogues of **3** on the basis of small model systems containing ammonia ligands and optimised only the ground state of the most stable conformers of **4**, **5** and **6**. The mononuclear $LCuO_2^+$ complex **4** has a $^3B$ ground state in $C_2$ symmetry and the $O_2$ group is coordinated side-on. The bis-peroxo form of the binuclear cluster **5** in $D_2$ symmetry has a singlet ground state. The tetranuclear complex **6** with $Cu_4(\mu\text{-}O)_2$-core has a Jahn–Teller unstable $^3E$ ground state in the $D_4$-symmetric conformation that distorts into $D_2$ symmetry. Calculations on the model complex $[\{Cu(NH_3)_2\}_4(\mu\text{-}O)_2]^{4+}$ (**9**) showed that the



0947-6539/98/0407-1300 $ 17.50+.50/0 *Chem. Eur. J.* **1998**, *4*, No. 7

Jahn–Teller stabilisation is about 10 kJ mol$^{-1}$, although it involves significant changes in the Cu–Cu distances. We optimised the geometry of **6** in $D_4$ symmetry, since the benefit from doing the calculations in $D_2$ symmetry would not justify the cost. The most important structural parameters for **4**, **5** and **6** are listed in Table 3.

Table 3. Geometrical parameters [Å] of $[\{CuL\}_n(O_2)]^{n+}$, L = *N*-permethyl-(1*R*,2*R*)-cyclohexenediamine} $n = 1$, 2, and 4 ; (**4**, **5**, and **6**, respectively).

| | **4** | **5** | **6** |
|---|---|---|---|
| coordination mode | side-on | peroxo | oxo |
| symmetry | $C_2$ | $D_2$ | $D_4$ |
| electronic state | $^3$B | $^1$A | $^3$E |
| Cu1–Cu2 | – | 3.529 | 2.572 |
| Cu1–O | 1.986 | 1.923 | 2.140 |
| O–O | 1.327 | 1.527 | 2.256 |

**Population and charge analysis of $L_3Cu_3O_2^{3+}$**: The partial charges and net spin populations of copper and oxygen atoms from a Mulliken type population analysis of **7** are listed in Table 1. In addition we carried out a Hirshfeld charge analysis, which is a more realistic representation of the charge distribution in the molecule. The charges in the Hirshfeld analysis are weighted by the density of the contributing atoms or fragments.[33] This analysis allows one to calculate the net charge transferred between reactants by carrying out the analysis with the reactants as fragments. Applying this analysis to the $^3$B state of **3** in $C_2$ symmetry, the symmetry-unique and the symmetry-equivalent $LCu^I$ fragments donate 0.53 and 0.34 electrons per fragment, respectively, with the total of 1.2 electrons transferred to the $O_2$.

The Mulliken and the Hirshfeld charges on the oxygen of **7** are $-0.72$ and $-0.29$, respectively, and they are mostly independent of the electronic state. The Mulliken charges on the copper centres of **7** are between 0.77 and 0.96, while the Hirshfeld charges lie in a narrow range of 0.47 to 0.51. The spin population analysis shows that the net spin density is almost equally divided between the Cu and the O atoms in the triplet state. In the two $C_{2v}$-symmetric Jahn–Teller structures the symmetry-unique and the symmetry-equivalent copper atoms have distinctly different spin populations. In the $^3B_2$ state the spin population of the symmetry-unique atom is zero, while the symmetry-equivalent coppers have a net spin of 0.38. On the other hand, in the $^3A_1$ state the symmetry-unique copper has a large spin density of 0.44, whereas the symmetry-related copper atoms have a smaller spin density of 0.16.

**Binding energy decomposition of $L_2Cu_2O_2^{2+}$, $L_3Cu_3O_2^{3+}$ and $L_4Cu_4O_2^{4+}$**: More insight into the bonding can be gained through a bond analysis developed by Ziegler and Rauk[34] based on a breakdown of the binding energy into different components. Jacobsen et al. applied this approach successfully to other bridged metal complexes.[35] Although this procedure is quite mathematical, the aim is to explain bonding in three simple terms: orbital interaction energies ($\Delta E_{el}$), steric interaction ($\Delta E^0$) and preparation energy ($\Delta E_{prep}$) [Eq. (1)].

$$\Delta E_{binding} = \Delta E_{el} + \Delta E^0 + \Delta E_{prep} \quad (1)$$

The binding energy ($\Delta E_{binding}$) in our calculations represents the reaction energy of dioxygen addition to one, two, three or four $Cu^IL$ fragments; the corresponding results are summarised in Table 4. The term $\Delta E_{el}$ represents the main features of the common theory by Parr and Pearson in which the binding energy is related to the differences in electronegativity and hardness between interacting fragments.[36] The electronic contributions in our system arise from the donation of copper d electrons into the $\pi^*$ and $\sigma^*$ orbitals on the oxygen. The steric interaction term arises from the competing attractive Coulomb electrostatic and the dominating repulsive Pauli interactions. The preparation energy reflects the rigidity of the ligands. This energy is required for the deformation of the separated fragments from their initial equilibrium position to the conformation in the final complex. The deformation energy includes the energetic cost of stretching the O–O bond of dioxygen to the O–O distance in the final complex; we have included this separately from the ligand deformation energy in Table 4.

In Table 4, we listed the important contributions to the binding energies of mono-, bi- tri-, and tetranuclear $L_nCu_nO_2^{n+}$ clusters including two isomers of a binuclear cluster with triazacyclononane-supporting ligands (**10A** and **10B**) from previous calculations.[13] The ligand preparation energy represents a relatively small contribution to the total binding energy; this means that the ligands are already constrained in the reactants to a conformation close to that found in the

Table 4. Binding energy decomposition [kJ mol$^{-1}$].[a]

| | **4** | **10A** | **5** | **10B** | **3** | **7** | **6** |
|---|---|---|---|---|---|---|---|
| symmetry | $C_2$ | $C_{2h}$ | $D_2$ | $C_{2h}$ | $D_3$ | $D_3$ | $D_4$ |
| ligand coordination | bidentate | tridentate | bidentate | tridentate | bidentate | bidentate | bidentate |
| $O_2$ coordination | peroxo | peroxo | peroxo | $(\mu\text{-O})_2$ | $(\mu\text{-O})_2$ | $(\mu\text{-O})_2$ | $(\mu\text{-O})_2$ |
| $\Delta E_{prep}$ ligand | 9 | 17 | 24 | 60 | 18 | N/A | 41 |
| $\Delta E_{prep}$ $O_2$ | 22 | 100 | 147 | – | 616 | 634 | 597 |
| Electronic contributions ($\Delta E_{el}$) | | | | | | | |
| $\sigma^* + \pi^*$ | $-310$ | $-610$ | $-827$ | $-1601$ | $-2007$ | $-1896$ | $-2233$ |
| Steric interactions ($\Delta E^0$) | | | | | | | |
| Pauli repulsion | 398 | 812 | 1073 | 1778 | 1877 | 1797 | 1625 |
| Coulomb electrostatic | $-252$ | $-291$ | $-369$ | $-800$ | $-258$ | $-282$ | 192 |

[a] $\Delta E$ corresponding to $nCu^IL + O_2 \rightarrow L_nCu_nO_2$. Only the terms discussed in the text are listed. Calculations on **10A** and **10B** from ref. [13]. See Schemes 1 and 2 for numbering of systems.

products. The same is not true for model systems with ammonia ligands, which lack the proper geometrical constraint to represent the ligand conformation energies, but are successful in reproducing the other energy terms. The $O_2$ preparation energy is significantly higher for the oxo isomers than for the peroxo isomers; this indicates that it takes more energy to break the O–O bond of dioxygen than to elongate it to a peroxide bond length. As we have previously shown, with the examples of **10A** and **10B**, the $(\mu\text{-O})_2$ isomers have more attractive orbital interactions than the $(\mu\text{-}\eta^2\text{:}\eta^2\text{-O}_2)$ isomer. These interactions are offset by the energetic cost of breaking the O–O bond and by the more repulsive steric interactions of the $(\mu\text{-O})_2$ isomer.[13] The formation of the $(\mu\text{-O})_2$ clusters requires the breaking of the O–O bond by electron donation into the σ* orbital, whereas the σ* interaction energy of the $(\mu\text{-}\eta^2\text{:}\eta^2\text{-O}_2)$ isomer is insignificant. In order to study trends with respect to cluster size one has to treat the peroxo and the oxo isomers separately; this limits the comparison to two pairs, the mono- and binuclear peroxo complexes, and the tri- and tetranuclear oxo complexes. Within this limited sample the orbital interaction energies are somewhat more attractive, but the steric interaction energies are more repulsive with increasing cluster size. Both the Pauli and Coulomb interactions become more repulsive (or less attractive) as the number of copper atoms in the coordination sphere increases.

To calculate the relative stabilities of different cluster sizes, we need to calculate reaction energies relative to a given amount of limiting reagent, the $Cu^{I}L$ complex. Accordingly, the overall reaction energies of $Cu^{I}L + 1/n\,O_2 \rightarrow 1/n\,L_nCu_nO_2$ reactions for the mono-, bi-, tri- and tetranuclear clusters **4**, **5**, **3** and **6** are −117, −74, −10 and +171 kJ mol$^{-1}$, respectively. The reaction energy of the $(\mu\text{-}\eta^3\text{:}\eta^3\text{-O}_2)$ isomer of **3** is 162 kJ mol$^{-1}$ above that of the $(\mu\text{-O})_2$ isomer.

**Solvation energies and relative stabilities**: We calculated the solvation energies of the reactants and the products of the self-assembly reactions using a dielectric constant of 9.2 and a probe radius of 2.8 Å in the dielectric-continuum calculations, which correspond to the $CH_2Cl_2$ solvent of the experiment that yielded **3**.[8] The calculated solvation energies of the reactant **11**, and the mono- bi-, tri- and tetranuclear products (**4**, **5**, **3**, and **6**) are −166, −172, −472 −946 and −1544 kJ mol$^{-1}$, respectively. The contribution from the solvation energy to the reaction energy for the formation **4**, **5**, **3** and **6**, from one mole of mononuclear complex **11**, is −6, −70, −149 and −220 kJ, respectively. The combined quantum-mechanical binding and solvation energies of formation of **4**, **5**, **3** and **6** and are −123, −144, −159 and −49 kJ mol$^{-1}$, respectively, relative to one mole of mononuclear complex.

The two Jahn–Teller components of **7** and **3** have different charge distributions, which may lead to different solvation energies. The calculated solvation energies of the $^3$B and $^3$A Jahn–Teller components of model complex $[L_3Cu_3O_2]^{3+}$ (L = (1*R*,2*R*)-cyclohexene-diamine, **8**) were 1057 and 1062 kJ mol$^{-1}$, respectively. While solvation makes the $^3$A state lower in energy by 5 kJ mol$^{-1}$, the gas-phase bonding energy favours the $^3$B state by only 0.5 kJ mol$^{-1}$.

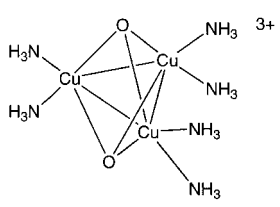


**7**

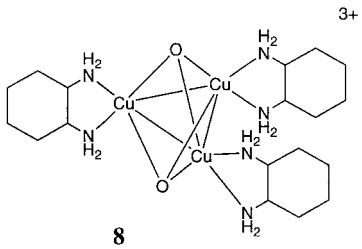


**8**

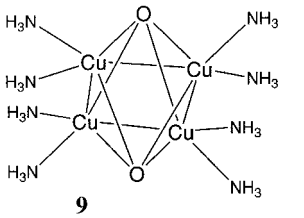


**9**

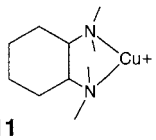


**11**

## Discussion

The calculated core geometry of the various conformations and states of **7** can be compared with the experimentally determined X-ray structure of **3** (Table 1). One of the $C_{2v}$-symmetric Jahn–Teller components of the lowest energy state, the $^3B_1$ state, has a geometry with a pair of short and two pairs of long Cu–O bonds that corresponds to the observed core structure of **3**.

The two calculated symmetry-inequivalent Cu–O bond lengths are close to the experimental values, although the calculation underestimates the anisotropy. The differences in the inequivalent Cu–O bond distances are 0.17 and 0.10 Å in the observed and calculated structures, respectively.

The calculated and experimental distances of the shorter Cu–O bond are 1.83 and 1.90 Å, respectively. Such short Cu–O bond lengths have been found in solid-state materials, such as $KCuO_2$, and recently in the $Cu_2(\mu\text{-O})_2$-core isomer of **1** (**1B**). The oxidation state of copper in such complexes has been characterised as $Cu^{III}$. The longer Cu–O bonds are 2.00 Å as determined both by experiment and calculations; this is a typical bond length for $Cu^{II}$–O systems. One may conclude from these structural data that **7** and **3** are mixed-valent compounds, with $Cu^{III}Cu^{II}Cu^{II}$ oxidation states.[8] The Mulliken charges on the symmetry-unique and the symmetry-related copper atoms of the $^3B_2$ state of **7** and that of the isolated $Cu^{I}L$ fragment are 0.96, 0.77 and 0.55, respectively. Accordingly, twice as much charge is transferred to the symmetry-unique copper atom than to the symmetry-equivalent ones.

The Hirshfeld analysis of the $^3$B state of **3** supports the anisotropic charge transfer of 0.53 and 0.34 electrons from the symmetry-unique and the symmetry-equivalent $LCu^{I}$ fragments, respectively. The net spin population of the symmetry-unique copper in the $^3B_2$ state is almost zero and that of the two other coppers is 0.4. These findings are consistent with the previous characterisation of **3** as a mixed-valence $Cu^{III}Cu^{II}Cu^{II}$ cluster in a triplet state due to the parallel alignment of the spins of the symmetry-related copper atoms.[8] However, one should not read too much significance into these qualitative descriptions based on integer oxidation numbers or conclude that the fourth electron is supplied by the



0947-6539/98/0407-1302 $ 17.50+.50/0 *Chem. Eur. J.* **1998**, *4*, No. 7

symmetry-unique $Cu^{III}$ atom. The other Jahn–Teller component of the same system could not be properly described with integers for the oxidation states of copper. The larger charge transfer from the symmetry-unique atom of the $^3B_2$ state of **7** is a consequence of Jahn–Teller distortion. These calculations predict that the Jahn–Teller stabilisation energy is only 6 kJ mol$^{-1}$, thus the two Jahn–Teller components are in equilibrium in solution. The calculation indicates a high degree of covalency between copper and oxygen for both isomers, and thus explains why the formal oxidation states and calculated charges are so different. Therefore, **7** and **3** are best described as Jahn–Teller distorted, average valence, highly polarised, covalent compounds.

Our calculations on the model system **8**, in which the methyl groups are replaced by hydrogens, predict that the energies of the two Jahn–Teller components are within 0.5 kJ mol$^{-1}$ in favour of the $^3B$ state, whereas solvation energy favours the $^3A$ state by 5 kJ mol$^{-1}$. It is not contradictory that the crystal geometry preferred is the $^3B$ state, since crystal packing forces can make a significant energetic difference between the two isomers.

The self-assembly synthesis of $M_nO_2$ complexes can yield a variety of different cluster sizes and core isomers depending on the coordinating ligand and the solvent. The substituted tridentate 1,4,7-triazacyclononane (tacn) and pyrazolyl borate [$HB(pz)_3$] ligands yielded the binuclear products, **1** and **2**, on coordination to $Cu^I$[3, 4, 5] (represented by **10** and **12** in the calculations[12]) whereas coordination of the bidentate 1,2-cyclohexanediammine (1,2-CHDA) ligand preferentially produced the trinuclear compound **3**.[7] The reaction yielding **3** was very sensitive to temperature and solvent. Similarly, solvation effects determined which of the core isomers of **1** was formed (Scheme 1). To understand these factors we first discuss the gas-phase binding energies of binuclear and trinuclear clusters studied here and in our previous work. The most strongly bound binuclear complex is **12** with the $HB(pz)_3$ ligand ($-90$ kJ mol$^{-1}$) followed by **5** ($-74$ kJ mol$^{-1}$), **10 A** ($-30$ kJ mol$^{-1}$) and then the least strongly bound cluster **3** ($-10$ kJ mol$^{-1}$) relative to one mole of $Cu^IL$. We explained the increased stability of **12** by charge stabilisation of the negatively charged hydride. On the other hand **5** and **10 A,** which are both binuclear, peroxo-coordinated and have neutral ligands, differ only in their ligand-coordination modes. The orbital interactions of **5** with bidentate ligands are stronger ($-827$ kJ mol$^{-1}$) than those of **10 A** with tridentate ligands ($-610$ kJ mol$^{-1}$). Although this effect is partially compensated by the stronger steric repulsion, the bidentate supporting ligand is more energetically favourable than the tridentate one.

Some structural data from enzymes and their mimics are consistent with a preferred bidentate coordination in $Cu_2O_2N_6$-coordinated clusters. The apical Cu–N bonds of $Cu_2O_2N_6$ systems are always longer than equatorial Cu–N bonds, an indication that the third apical ligand is less strongly bound than the equatorial ones. Upon dioxygen binding, the apical Cu–N distance of the active site of oxyhemocyanin increases from 2.2 to 2.7 Å, which essentially switches the tridentate to bidentate coordination.[1, 2] In biological systems the coordination of three *N* donors to copper is versatile and the apical ligand can be used for fine-tuning the energetic balance of $O_2$ binding.

Comparison of the mono-, bi-, tri- and tetranuclear clusters **4**, **5**, **3** and **6** shows that the gas-phase stability decreases with increasing size. When solvation-energy contributions are added to the gas-phase binding energies the energetic ordering changes in favour of the trinuclear cluster. The preference for the formation of the trinuclear cluster is controlled entirely by solvation effects that compensate for the unfavourable electronic and steric effects. The strong solvation effects can be predicted based on the Born formula of solvation free energy [Eq. (2)].

$$\Delta G_{solv} = -\frac{Q^2}{2R}\left(1-\frac{1}{\varepsilon_0}\right) \quad (2)$$

From Equation (2) it can be seen that solvation effects will be much more favourable for increased cluster size when the metal centres are charged. As a consequence, the solvation energies can compensate for the loss of binding energy as the size of the cluster increases.

Considering the experimentally found inorganic $Cu_3O_2$ cluster and the hypothetical trinuclear intermediate in ascorbate oxidase, these two systems differ both in ligand coordination and solvation effects. Two of the three copper atoms at the active site of ascorbate oxidase have tridentate coordination, and we found that bidentate coordination was preferred in binuclear clusters and this, most likely, is also true for trinuclear analogues. The active site of these enzymes is accessible to a few water molecules, but the protein shields the active site from continuum solvation effects. How water coordination changes the energetics could not be derived from the present results. Another factor to consider is the availability of protons that may prevent the formation of the trinuclear oxo complex in favour of the analogous hydroxo product. When traces of water are present in the reaction yielding **3**, the thermodynamic product is the binuclear hydroxo compound.[8] Based on the present results it is unlikely that the $Cu_3O_2$ core is a stable intermediate in biological systems, which may explain why it has not been observed.

## Conclusions

The electronic structure of the $Cu_3(\mu\text{-}O)_2$ chromophore can be best described as a Jahn–Teller distorted, average valence, highly polarised, covalent system. The two Jahn–Teller components are predicted to be in equilibrium in solution, separated by only a modest 6 kJ mol$^{-1}$ barrier. The preference for the $^3B$ state in the crystal structure must be related to crystal packing forces, which are beyond the capability of our molecular modelling tools. The formation energy of $Cu_n-O_2$ clusters in the gas phase decreases significantly with increasing cluster size, but solvation energy has the opposite trend of similar magnitude. As a consequence of these competing effects, the relative stabilities of clusters with mono-, bi- and trinuclear cores differ only by a few tens of kJ mol$^{-1}$ in $CH_2Cl_2$. The self-assembly formation of the $Cu_3O_2$ cluster under experimental conditions is controlled entirely by

solvation effects, and the mono- or binuclear analogue would be favoured in the gas phase or in a low-dielectric solvent. These calculations demonstrate that the thermodynamic product of charged clusters in solution is determined by two large, competing effects: solvation and binding energies. Since the protein environment of the enzyme shields the active site from continuum solvation effects, the relevance of the thermodynamic products of solution chemistry in biological systems remains to be established.

**Acknowledgements**: I thank several colleagues who provided software, assistance, opinion and criticism related to this study: Professor Peter Pulay provided the INTC program used to generate the input for natural coordinate optimisation; Dr. Don Bashford made the MEAD program available that was used in the solvation energy calculation; Drs. Louis Noodleman, David Case and Jian Li introduced me to solvation energy calculation and discussed many aspects of electronic structures of metal clusters; my colleagues at the Steacie Institute provided their opinion and constructive criticism of this manuscript. I gratefully acknowledge a visiting fellowship from the National Research Council Canada. This paper is issued as NRCC# 40861.

Received: January 8, 1998 [F956]

[1] a) K. Magnus, H. Ton-That, J. E. Carpenter, in *Bioinorganic Chemistry of Copper* (Eds.: K. D. Karlin, Z. Tyeklar), p. 143, Chapman and Hall, New York, **1993**; b) K. Magnus, H. Ton-That, J. E. Carpenter, *Proteins: Struct. Funct. Genet.* **1994**, *19*, 302.

[2] A. Volbeda, G. J. Hol, *J. Mol. Biol.* **1989**, *209*, 249.

[3] a) S. Mahapatra, J. A. Halfen, E. C. Wilkinson, G. Pan, C. J. Cramer, L. Que, Jr., W. B. Tolman, *J. Am. Chem. Soc.* **1995**, *116*, 9785; b) S. Mahapatra, J. A. Halfen, E. C. Wilkinson, G. Pan, C. J. Cramer, L. Que, Jr., W. B. Tolman, *ibid.* **1995**, *117*, 8865.

[4] a) N. Kitajima, T. Koda, S. Hashimoto, T. Kitagawa, Y. Moro-oka, *J. Chem. Soc. Chem. Commun*. **1988**, 151; b) N. Kitajima, K. Fujisawa, Y. Moro-oka, K. Toriumi, *J. Am. Chem. Soc.* **1989**, *111*, 8975.

[5] J. A. Halfen, S. Mahapatra, E. C. Wilkinson, S. Kaderli, V. G. Young, Jr., L. Que, Jr., A. D. Zuberbühler, W. B. Tolman, *Science* **1996**, *271*, 1397.

[6] a) D. M. Proserpio, R. Hoffman, G. C. Dismukes, *J. Am. Chem. Soc.* **1992**, *114*, 4374; b) A. L. Feig, S. J. Lippard, *Chem. Rev.* **1994**, *94*, 759; c) V. L. Pecoraro, M. J. Baldwin, A. Gelasco, *Chem. Rev.* **1994**, *94*, 807.

[7] A. P. Cole, D. E. Root, P. Mukherjee, E. I. Solomon, T. D. P. Stack, *Science* **1996**, *273*, 1849.

[8] a) D. J. Spira-Solomon, M. D. Allendorf, E. I. Solomon, *J. Am. Chem. Soc.* **1986**, *108*, 5318; b) A. Messerschmidt, R. Ladenstein, R. Huber, M. Bolognesi, L. Avigliano, R. Petruzzelli, A. Rossi, A. Finazzi-Agro, *J. Mol. Biol.* **1992**, *224*, 179; c) A. M. D. Llendorf, D. J. Spira, E. I. Solomon, *Proc. Nat. Acad. Sci. U.S.A.* **1985**, *82*, 3063; d) L. Ryden, I. Björk, *Biochemistry* **1976**, *15*, 3411; e) I. Zajtseva, V. Zaitsev, G. Card, K. Moshkov, B. Box, A. Ralp, P. Lindley, *J. Biol. Inorg. Chem.* **1996**, *1*, 15; f) A. Messerschmidt, H. Luecke, R. Huber, *J. Mol. Biol.* **1993**, *230*, 997; g) J. L. Cole, P. A. Clark, E. I. Solomon, *J. Am. Chem. Soc.* **1990**, *112*, 9534.

[9] a) A. Messerschmidt, R. Ladenstein, R. Huber, M. Bolognesi, L. Avigliano, R. Petruzzelli, A. Rossi, A. Finazzi-Agro, *J. Mol. Biol.* **1992**, *224*, 179; b) I. Zaitseva, V. Zaitsev, G. Card, K. Moshov, B. Bax, A. Ralph, P. Lindely, *J. Biol. Inorg. Chem.* **1996**, *1*, 15; c) A. Messerschmidt, R. Huber, *Eur. J. Biochem.* **1990**, *187*, 341; d) L. G. Ryden, L. T. Hunt, *J. Mol. Evol.* **1993**, *36*, 41.

[10] E. I. Solomon, U. M. Sundaram, T. E. Machokin, *Chem. Rev.* **1996**, *96*, 2563.

[11] T. Ziegler, *Chem.Rev.* **1991**, *91*, 651.

[12] a) A. Bérces, *Inorg. Chem*. **1997**, *36*, 4831; b) A. Bérces, *Int. J. Quantum Chem.* **1997**, *65*, 1077.

[13] a) P. K. Ross, E. I. Solomon, *J. Am. Chem. Soc.* **1990**, *112*, 5871; b) P. K. Ross, E. I. Solomon, *ibid.* **1991**, *113*, 3246; c) F. Tuczek, E. I. Solomon, *ibid.* **1994**, *116*, 6916; d) C. J. Cramer, B. A. W. B. Smith, Tolman, *ibid.* **1996**, *118*, 11283.

[14] E. J. Baerends, D. E. Ellis, P. Ros, *Chem.Phys.* **1973**, *2*, 41.

[15] a) W. Ravenek, in *Algorithms and Applications on Vector and Parallel Computers* (Eds: H. J. J. te Riele, Th. J. Dekker, H. A. van de Vorst), Elsevier, Amsterdam, **1987**; b) P. M. Boerrigter, G. te Velde, E. J. Baerends, *Int. J. Quantum Chem.* **1988,** *33*, 87; c) G. te Velde, E. J. Baerends, *J. Comp. Phys.* **1992**, *99*, 84.

[16] a) L. Fan, T. Ziegler, *J. Chem. Phys.* **1991**, *94*, 6057; b) L. Fan, T. Ziegler, *ibid.* **1991**, *95*, 7401; c) L. Fan, L. Versluis, T. Ziegler, E. J. Baerends, W. Ravenek, *Int. J. Quantum Chem.* **1988,** *S22*, 173; d) L. Fan, T. Ziegler, *J. Chem. Phys.* **1992,** *96*, 9005; e) L. Fan, T. Ziegler, *J. Phys. Chem.* **1992**, *96*, 6937.

[17] a) S. H. Vosko, L. Wilk, M. Nusair, *Can. J. Phys.* **1980**, *58*, 1200; b) A. D. Becke, *Phys. Rev*. A **1988,** *38*, 2398; c) J. P. Perdew, *Phys. Rev.* B **1986,** 33, 8822; d) J. P. Perdew, *ibid.* **1986**, *34*, 7046.

[18] a) J. G. Snijders, E. J. Baerends, P. Ros, *Mol. Phys.* **1978**, *36*, 1789; b) J. G. Snijders, E. J. Baerends, P. Ros, *ibid.* **1979**, *36*, 1969.

[19] G. Schreckenbach, T. Ziegler, J. Li, *Int. J. Quantum Chem. Quantum Chem. Symp.* **1995**, *56*, 477.

[20] a) P. Császár, P. Pulay, *J. Mol. Struct.* **1984**, *114*, 31; b) P. Pulay, *Chem. Phys. Lett.* **1980**, *73*, 393; c) P. Pulay, *J. Comput. Chem.* **1982**, *3*, 556.

[21] a) G. Fogarasi, X. Zhou, P. W. Taylor, P. Pulay, *J. Am. Chem. Soc.* **1992**, *114*, 8191; b) P. Pulay, G. Fogarasi, F. Pang, J. E. Boggs, *ibid.* **1979**, *101*, 2550.

[22] Programmed by A. G. Csaszar, P. G. Szalay, Eötvös University, Budapest (Hungary), **1984**.

[23] a) A. Bérces, *J. Comp. Chem.* **1997**, *18*, 4555; b) A. Bérces, T. Ziegler, *J. Phys. Chem.* **1994**, *98*, 13233; c) A. Bérces, T. Ziegler, L. Fan, *ibid.* **1994**, *98*, 1584.

[24] INTC program to generate natural internal coordinates, P. Pulay, G. Fogarasi, Univerity of Arkansas, Fayetteville, **1992**.

[25] a) G. J. Snijders, E. J. Baerends, P. Vernooijs, *Atomic Nuclear Data Tables* **1982**, *26*, 483; b) P. Vernooijs, G. J. Snijders, E. J. Baerends, *Slater Type Basis Functions for the Whole Periodic System*, internal report, Free University of Amsterdam, (The Netherlands), **1981**.

[26] J. Krijn, E. J. Baerends, *Fit Functions in the HFS-Method*, unternal report (in Dutch), Free University of Amsterdam (The Netherlands), **1984**.

[27] T. Ziegler, *Chem. Rev.* **1991**, *91*, 651.

[28] C. M. Breneman, K. B. Wiberg, *J. Comput. Chem.* **1990**, *11*, 361.

[29] a) D. Bashford, *Curr. Opin. Struct. Biol.* **1991**, *1*, 175; b) D. Bashford, K. Gerwert, *J. Mol. Biol.* **1992**, *224*, 473; c) C. Lim, D. Bashford, M. Karplus, *J. Phys. Chem.* **1991**, *95*, 5610; d) D. Bashford, D. A. Case, C. Dalvit, L. Tennant, P. E. Wright, *Biochemistry* **1993**, *32*, 8045.

[30] a) L. Noodleman, *J. Chem. Phys.* **1981**, *74*, 5737; b) E. A. Schmitt, L. Noodleman, E. J. Baerends, D. N. Handrickson, *J. Am. Chem. Soc.* **1992**, *114*, 6109; c) J.-M. Mouesca, L. Noodleman, D. A. Case, *Inorg. Chem.* **1994**, *33*, 4819; d) J.-M. Mouesca, J. L. Chen, L. Noodleman, D. Bashford, D. A. Case, *J. Am. Chem. Soc.* **1994**, *116*, 11898; e) L. Noodleman, D. A. Case, *Adv. Inorg. Chem.* **1992**, *38*, 423-470; f) L. Noodleman, E. J. Baerends, *J. Am. Chem. Soc.* **1984**, *106*, 2316.

[31] T. A. Albright, J. K. Burdett, M.-H. Whangbo, *Orbital Interactions in Chemistry*, Wiley, New York, **1985**.

[32] a) S. Mahapatra, J. A. Halfen, E. C. Wilkinson, G. Pan, X. Wang, V. G. Young, Jr., C. J. Cramer, L. Que, Jr., W. B. Tolman, *J. Am. Chem. Soc.* **1996**, *118*, 11555; b) C. J. Cramer, B. A. Smith, W. B. Tolman, *ibid.* **1996**, *118*, 11283; c) B. A. Smith, C. J. Cramer, *ibid.* **1996**, *118*, 5490; d) S. Mahapatra, J. A. Halfen, E. C. Wilkinson, G. Pan, C. J. Cramer, L. Que, Jr., W. B. Tolman, *ibid.* **1995**, *117*, 8865.

[33] a) F. L. Hirshfeld, *Theoret. Chim. Acta* **1977**, *44*, 129; b) K. B. Wiberg, P. R. Rablen, *J. Comp. Chem.* **1993**, *14*, 1504.

[34] a) T. Ziegler, A. Rauk, *Theor. Chim. Acta* **1977**, *46*, 1; b) T. Ziegler, *A General Energy Decomposition Scheme for the Study of Metal–Ligand Interactions in Complexes, Clusters and Solids*, NATO ASI, in press; c) T. Ziegler, A. Rauk, *Inorg. Chem*. **1979**, *18*, 1558; d) T. Ziegler, A. Rauk, *ibid*. **1979**, *18*, 1755.

[35] H. Jacobsen, H.-B. Kraatz, T. Ziegler, M. P. Boorman, *J. Am. Chem. Soc*. **1992**, *114*, 7851.

[36] a) R. G. Pearson, *Inorg. Chem*. **1988**, 27, 734; b) R. E. Parr, R. G. Pearson, *J. Am. Chem. Soc*. **1983**, *105*, 7512.

  0947-6539/98/0407-1304 $ 17.50+.50/0 